PTEP

Prog. Theor. Exp. Phys. **2018**, 103A02 (16 pages)
DOI: 10.1093/ptep/pty099

Mixed-mode oscillation-incrementing bifurcations and a devil's staircase from a nonautonomous, constrained Bonhoeffer–van der Pol oscillator

Hiroaki Takahashi[1], Takuji Kousaka[2,*], Hiroyuki Asahara[3], Nataliya Stankevich[4,5,6], and Naohiko Inaba[7]

[1]*Department of Mechanical and Energy System Engineering, Oita University, Oita 870-1192, Japan*
[2]*Department of Electrical and Electronic Engineering, Chukyo University, Nagoya 466-8666, Japan*
[3]*Department of Electrical and Electronic Engineering, Okayama University of Science, Okayama 700-0005, Japan*
[4]*Department of Radioelectronics and Communications, Yuriy Gagarin State Technical University of Saratov, Politehnicheskaya 77, Saratov 410054, Russia*
[5]*Kotel'nikov's Institute of Radio-Engineering and Electronics of RAS, Saratov Branch, Zelenaya 38, Saratov 410019, Russia*
[6]*Faculty of Information Technology, University of Jyväskylä, FI-40014 Jyväskylä, Finland*
[7]*Organization for the Strategic Coordination of Research and Intellectual Properties, Meiji University, Kawasaki 214-8571, Japan*
[*]E-mail: takuji@bifurcation.jp

Received April 13, 2018; Revised July 13, 2018; Accepted August 7, 2018; Published October 26, 2018

In this study, we analyze mixed-mode oscillation-incrementing bifurcations (MMOIBs) generated in the nonautonomous, constrained Bonhoeffer–van der Pol oscillator proposed by Kousaka et al. [Physica D **353–354**, 48 (2017)]. Specifically, we investigate MMOIBs occurring in the 1^4–1^5 and 1^1–1^2 regions. These two kinds of MMOIBs exhibit qualitatively different MMO-bifurcation structures. The former MMOIBs successively occur many times, while the latter exhibit finite MMOIBs. In the latter case, standard MMOIBs occur only five times, and are then followed by another type of MMOIB. However, the following MMOIBs are also only generated seven times and the solution finally settles down into a 2^0 attractor. We clarify the exact reason for these phenomena by analyzing 1D Poincaré return maps derived from the constrained dynamics. By focusing on the initial successive MMOIBs, we create asymmetric Farey trees that occur between 1^4 and 1^5 by analyzing the 1D Poincaré return map. We find that there exist two sets of successive MMOIBs between 1^4 and 1^5. In particular, we rigorously define the MMO increment-terminating tangent bifurcations, toward which the MMOIBs accumulate and terminate. Furthermore, we uncover a nested bifurcation structure caused by MMOIBs. This occurs inside a short interval in the 1^4–1^5 region and accumulates toward another MMO increment-terminating tangent bifurcation point. These three types of successively generated MMOIBs accumulate in different ways toward the MMO increment-terminating tangent bifurcation points. We also analyze the behavior of the "firing number," which varies with the MMOIBs. In particular, we theoretically explain why a firing number that exhibits a devil's staircase has higher values in chaos-generating regions than in MMO-generating regions.

Subject Index A33

1. Introduction

Mixed-mode oscillations (MMOs) are a phenomenon first discovered in chemical experiments [1,6–8]. They comprise L large excursions and s small peaks, and such waveforms are symbolized by the notation "L^s." At an earlier stage, MMOs were also seen as "*alternating periodic and chaotic sequences*" [3]. At first, the definition of an MMO appears to be ambiguous. However, ever since it has been accepted that interesting MMO behaviors can be observed in extended slow/fast dynamics that can generate canards [1,10,12,16], MMOs of this type have generated intense research interest [2–5,12–26,29–35].

Kawczýnski et al. [15] found MMO-adding sequences that are generated by a simple, three-variable, slow/fast, autonomous ordinary differential equation (ODE). Shimizu et al. found similar bifurcations in a forced Bonhoeffer–van der Pol (BVP) circuit and termed the resulting bifurcation phenomena "mixed-mode oscillation-incrementing bifurcations" (MMOIBs) [17]. The simplest MMOIBs generate the MMO sequence $1^s(1^{s+1})^n$ for successive n. For example, the MMO sequence $1^2(1^3)^3$ represents $1^2 1^3 1^3 1^3$. MMOIBs are well known to occur in autonomous [5,15] and nonautonomous [22,23] chemical oscillators. Kawczýnski et al. [15], Shimizu et al. [19], and Kousaka et al. [20] found that MMOIBs occur in a manner similar to that of the period-adding bifurcations generated by a circle map. MMOIBs have been experimentally observed since the late 20th century, notably in chemical processes, such as the Belouzov–Zhabotinskii (BZ) [6,8] and the chlorite–thiosulfate reactions [7], as well as in electrochemical systems [9]. MMOIBs are known to be governed by Farey arithmetic [5,6,8,9,12].

However, rigorous analysis of MMOs and MMOIBs in real physical systems is usually extremely difficult because the smallest systems that exhibit MMOs and chaos are two-variable nonautonomous or three-variable autonomous ODEs. The bifurcations and chaos in such flows are conventionally analyzed using a mapping method, which converts the task of analyzing continuous dynamics into that of studying discrete mappings [11]. Such mappings are called Poincaré return maps. However, to generate chaos, such return maps must be at least 2D. Furthermore, analyzing discrete dynamical systems with two or more dimensions is known to be extremely difficult, even when the continuous chaos and MMO-generating dynamics to be analyzed are represented by extremely simple ODEs [10,11,48]. In contrast, 1D maps have been studied rigorously [55–60]. The mechanism responsible for generating chaos and tori in ODEs is considered to be quite simple, so similar bifurcation phenomena have been observed in 1D maps, such as the logistic [54,55] and circle [56,57] maps. With 1D maps, we can analyze various phenomena theoretically. With regard to MMOIB-related phenomena, period-adding and incrementing bifurcations have been analyzed using piecewise-linear and piecewise-smooth maps [64]. Moreover, recent research has focused on the gapping and overlapping of devil's staircase plateaus [61,62,64]. In addition, the structure of nested period-incrementing bifurcations has been analyzed using a three-segment piecewise-linear map [63].

Kousaka et al. [20] analyzed MMOIBs more rigorously using a nonautonomous constrained BVP oscillator that is defined when one of the parameters diverges. A 1D Poincaré return map can be derived from this constrained ODE. Such maps contain two convex downward branches in the invariant interval, which explain the successive MMOIBs. Their analysis may effectively fill the gap between experimental MMOIB observations and the results obtained for piecewise-smooth 1D maps [61,62,64]. Moreover, to investigate how many MMOIBs occur, Kousaka et al. attempted to derive a universal constant at which each MMOIB emerges. The constant appeared to converge to

unity, because the MMOIBs terminate by a saddle-node bifurcation [20], suggesting that MMOIBs can occur as many times as desired.

In this study, we investigate several MMOIBs using the constrained BVP oscillator proposed by Kousaka et al. [20]. We use the notation $[1^s, 1^{s+1} \times n]_m$ to represent the MMO sequence instead of $1^s(1^{s+1})^n$, where the subscript m represents the number of periods of the forcing term, because the dynamics is nonautonomous and the value of m must be specified. In simple MMOs, such as $[1^s, 1^{s+1} \times n]_m$, m is usually $m = n + 1$. We find two sets of successive MMOIBs between 1^5 and 1^4, and we illustrate the Farey trees that describe how the two sets of MMOIBs emerge. We assert that MMOIBs generate asymmetric Farey trees because the Poincaré return map contains two downward-convex branches. We believe that this is the first paper to clearly illustrate asymmetrical Farey trees based on a rigorous analysis of the 1D Poincaré return map. We define the MMO increment-terminating tangent bifurcations toward which the MMOIBs accumulate. It is noteworthy that the two sets of MMOIBs generated between 1^4 and 1^5 accumulate toward the MMO increment-terminating tangent bifurcation points in different manners. These results suggest that several different types of MMOIBs could exist. In addition, we uncover a nested MMOIB structure inside a short interval of the 1^4–1^5 region where the MMOs $[1^4, 1^5, [1^4, 1^5 \times 2] \times n]_{3n+2}$ emerge for successive n, and find another MMO increment-terminating tangent bifurcation point toward which the corresponding MMOIBs accumulate. We believe that this is one of the most significant results presented in this paper.

In addition, we investigate the bifurcation structure between 1^1 and 1^2, finding that the MMOIBs in this region are generated only a finite number of times. MMO bifurcations have been found to occur symmetrically in a surprising and unexpected way in both a three-variable BZ reaction model and an autocatalator model [26], forming Stern–Brocot trees, so we believe that finding a finite number of MMOIBs generated in a real physical system (which we show exactly) could be a significant result. Only five MMOIBs can occur when varying the bifurcation parameter between the branches generating 1^1 and 1^2, and they do not appear many times in succession. The flow must pass through the third branch of the 1D Poincaré return map generating 1^3, in addition to the branches generating 1^1 and 1^2, and the sequences $[1^1, 1^3, 1^1, 1^2 \times n]_{n+3}$ appear for n up to 12. Finally, when the bifurcation parameter is decreased further, the invariant interval that was present near the branches generating 1^1, 1^2, and 1^3 disappears, and the attractor transitions to $[2^0]_2$.

We also investigate the "firing number" F defined by $F = L_N/(L_N + s_N)$ where L_N and s_N represent the integer numbers of large excursions and small peaks, respectively, in one period of the MMO. It is known that—depending upon the value of the bifurcation parameter—the firing number can represent a devil's staircase [5,12,23,26]. Such devil's staircases are believed to represent stepwise functions [12]. They may appear because two separate neighboring MMOs generated by MMOIBs often overlap in parameter space due to hysteresis, and chaos rarely emerges between two neighboring MMOs in one-parameter bifurcation diagrams when n is large [12,15]. This phenomenon might be related to non-chaos-mediated MMOs, which have been recently discussed [27,28]. In contrast, in the nonautonomous BVP oscillator, chaos definitely emerges between two neighboring MMOs and the numerical results indicate that the firing number does not generate a stepwise function. Moreover, according to these results, the firing number F takes higher values than it does for periodic MMOs when the chosen bifurcation parameter values are in a chaos-generating region. We define 1^n to be shorter than 1^m if $n < m$. We theoretically explain the higher values of F in chaos-generating regions using a 1D Poincaré return map because the chaotic trajectories pass more often through the branches that generate shorter MMO sequences.

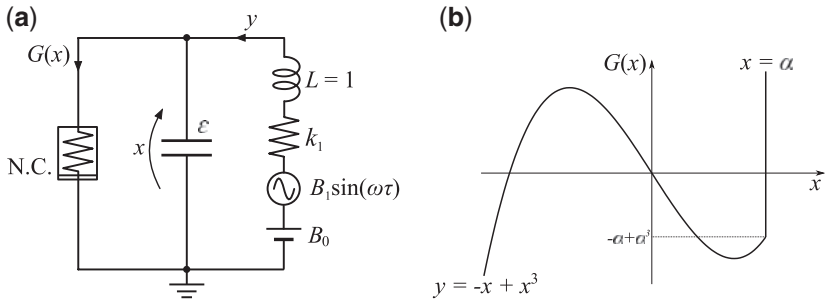

Fig. 1. (a) BVP oscillator under a weak periodic perturbation. (b) $v-i$ characteristic $G(x)$ of N.C.

2. Preliminary study

In this section, we recall the constrained, nonautonomous BVP oscillator discussed by Kousaka et al. [20]. The circuit diagram of the oscillator is presented in Fig. 1(a). In the figure, x and y are normalized variables corresponding to the voltage across the capacitor $C = \varepsilon$ and the current through the inductor L, respectively, where ε is assumed to be small. The value of L can be normalized to unity via rescaling. Figure 1(b) represents the $v-i$ characteristic $G(x)$ of the nonlinear conductance (N.C.). In the absence of perturbation, the BVP oscillator's bifurcation structure is richer than that of a van der Pol oscillator, even though it only consists of a linear resistor and an inductor in series. The van der Pol oscillator only exhibits a supercritical Hopf bifurcation, whereas the BVP oscillator can generate a subcritical Hopf bifurcation [65,66]. In the neighborhood of a subcritical Hopf bifurcation point, the BVP oscillator generates a bistability consisting of a stable focus and a stable relaxation oscillation, coexisting in close proximity in the x–y plane. Under a nonautonomous weak periodic perturbation, the BVP oscillator can exhibit extremely complex bifurcations, such as chaos disappearance [47] and MMOIBs [17,20], because the solution now alternates in a complex way between the focus and relaxation oscillation. Here, we consider a case wherein N.C. is completely saturated, with the threshold $x = \alpha$. A circuit element with such an idealized $v - i$ characteristic can easily be realized using bidirectionally connected diode arrays and a piecewise linear diode created using an operational amplifier [20]. The governing equation for the circuit can be expressed as the following nonautonomous, nonsmooth ODE:

$$1.\ \begin{cases} \varepsilon\dot{x} = y - G(x) \\ \dot{y} = -x - k_1 y + B_0 + B_1 \sin(\omega\tau) \end{cases} \text{, for piecewise linear diode OFF } (x < \alpha) \tag{1}$$

$$2.\ \begin{cases} x = \alpha \\ \dot{y} = -\alpha - k_1 y + B_0 + B_1 \sin(\omega\tau) \end{cases} \text{, for piecewise linear diode ON } (x = \alpha). \tag{2}$$

Note that x is constrained to take the value of $x = \alpha$ when the piecewise linear diode is ON, and the circuit equation (2) then reduces to a first-order equation because $x = \alpha$(=const.).

The solutions of these two equations are connected to each other if the following transition conditions hold: if $x < \alpha$ (OFF), the piecewise linear diode turns on when x increases to α. In contrast, if $x = \alpha$ (ON), the piecewise linear diode turns off when the current through the N.C. decreases to $-\alpha + \alpha^3$. In other words, the transition conditions are as follows:

$$1.\ \text{diode OFF } (1) \ \rightarrow\ 2.\ \text{diode ON } (2) : x = \alpha, \tag{3}$$

$$2.\ \text{diode ON } (2) \ \rightarrow\ 2.\ \text{diode OFF } (1) : y = -\alpha + \alpha^3. \tag{4}$$

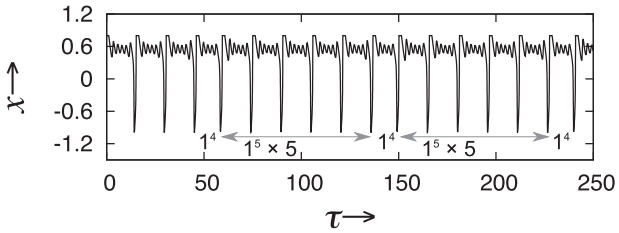

Fig. 2. Time series waveform of the MMO sequence $[1^4, 1^5 \times 5]_6$ after five MMOIBs for $\varepsilon = 0.1, k_1 = 0.9, B_0 = 0.207, B_1 = 0.01, \alpha = 0.8$, and $\omega = 0.4155$.

The solutions of Eqs. (1) and (2) are connected only for positive times based on Eqs. (3) and (4). Hence, the resulting Poincaré return map can become noninvertible and is 1D. Previous research [20] has shown that piecewise smooth dynamics that includes a piecewise linear diode captures the underlying mechanism that causes MMOs and MMOIBs. We consider this noninvertible dynamics here because real-world phenomena always proceed forward in time. Furthermore, the 1D Poincaré return map can well explain the phenomena observed in the real physical circuit [20]. We can justify analyzing simple 1D maps in such detail because the logistic and circle maps have played important roles in explaining the mechanisms behind period-doubling bifurcations [54,55,60] and torus breakdown [57].

Throughout this discussion, we set $\alpha = 0.8$. Figure 2 shows the waveform of an MMO after five MMOIBs. Here, the constant parameters were fixed as $\varepsilon = 0.1, k_1 = 0.9, B_0 = 0.207, B_1 = 0.01$, and $\alpha = 0.8$, and ω will be used as a bifurcation parameter in this study. The phenomena are extremely sensitive to the choice of fixed parameters because the stable focus and relaxation oscillation that coexist in the absence of perturbation only arise in a narrow parameter region. For example, if we instead select $B_0 = 0.21$, chaos disappearance occurs, but the bistability remains [47,48]. Here, chaos disappearance refers to the fact that the relaxation oscillation disappears under a very weak perturbation. Under such a perturbation, e.g., $B = 0.001$–0.03, the solution transitions to stay in close proximity to the stable focus that is present in the absence of perturbation. This phenomenon is so named because the relaxation oscillation is always chaotic immediately before it breaks down into an extremely weak periodic solution near the stable focus [47]. It is more prominent for smaller values of ε, and our numerical results reveal that it does not occur at $B_0 = 0.207$ for such a small B value. However, it is worth noting that MMOIBs have been observed in actual circuit experiments [18,20], although the phenomena are sensitive to the parameter values used.

As discussed in previous research [20], we define the following two objects:

$$\begin{aligned} \Pi_{\mathrm{r}} &= \{(\tau, x, y) | x - \alpha = 0\}, \\ \Sigma_1 &= \left\{(\tau, x, y) | x - \alpha = 0, y = -\alpha + \alpha^3\right\}, \end{aligned} \tag{5}$$

where Π_{r} is the plane in which the diode is ON and Σ_1 represents the transition condition 2. ON (2) $\rightarrow$ 1. OFF (1), which is located on plane Π_{r}. Figure 3 shows the geometric structure of the vector fields. Let us consider solutions that are initially located on Σ_1. Any solution leaving a point on Σ_1 eventually strikes Σ_1 again. Therefore, a 1D Poincaré return map that transforms an initial point ($\tau = \tau_0$) on Σ_1 to a point of Σ_1 ($\tau = \tau_1$) to which the solution leaving an initial point at $\tau = \tau_0$ returns is expressed as follows:

$$\begin{aligned} T: \quad & \Sigma_1 \rightarrow \Sigma_1, \\ & \theta_0 \mapsto \theta_1, \end{aligned} \tag{6}$$

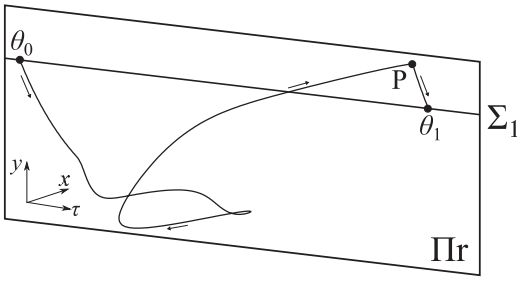

Fig. 3. Geometric structure of the vector fields.

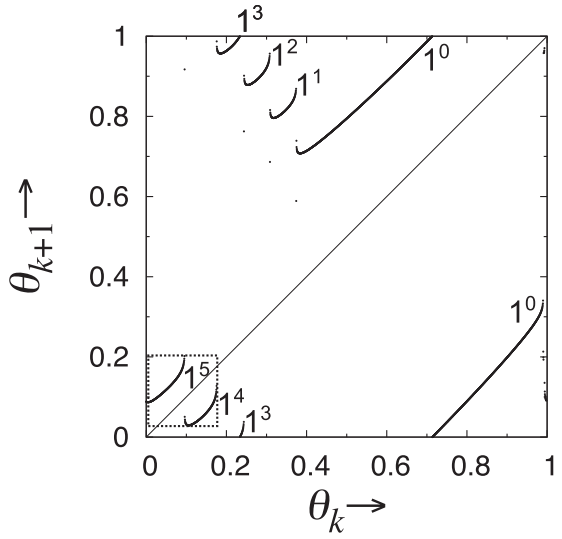

Fig. 4. 1D Poincaré return map for $\varepsilon = 0.1, k_1 = 0.9, B_0 = 0.207, B_1 = 0.01, \alpha = 0.8$, and $\omega = 0.434$.

where

$$\theta_0 = \frac{\omega\tau_0}{2\pi},\ \theta_1 = \frac{\omega\tau_1}{2\pi} \bmod 1. \tag{7}$$

Figure 4 shows an example of the 1D Poincaré return map that lies between the 1^4-generating region and the 1^5-generating region. In the figure, the pieces labeled by 1^0, 1^1, 1^2, ..., and 1^5 are branches that generate the MMO waveforms 1^0, 1^1, 1^2, ..., and 1^5, respectively.

3. One-parameter bifurcation diagrams and MMOIBs

Throughout this discussion, we fix the constant parameters at $\varepsilon = 0.1, k_1 = 0.9, B_0 = 0.207$, and $B_1 = 0.01$, as mentioned in the previous section, and we choose the angular frequency ω of the forcing term as the bifurcation parameter. Figure 5 shows a global view of the one-parameter bifurcation diagram for varying ω, where we have adopted a stroboscopic Poincaré section and the corresponding y values are plotted for large k. In the figure, the label 1^s indicates the region where the MMO sequence 1^s is generated. In this study, we concentrate on the regions that generate complex MMOs and MMOIBs between 1^5 and 1^4 and between 1^2 and 1^1. These two regions generate qualitatively different MMOIBs. When an MMOIB is generated, an invariant interval appears at the bottom left of the θ_k–θ_{k+1} plane of the 1D Poincaré return map, as shown in Fig. 4. While the former

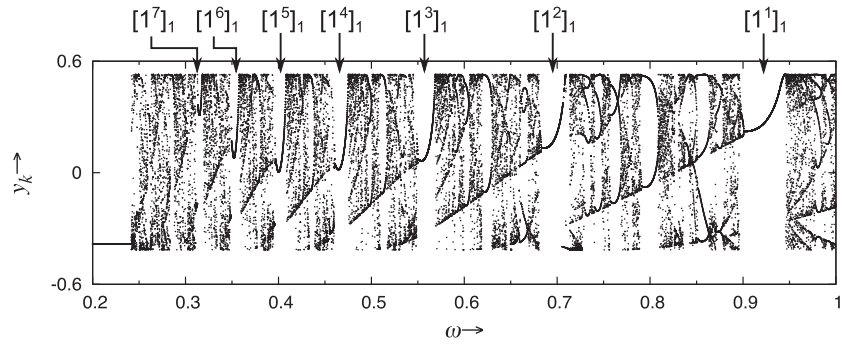

Fig. 5. Global view of the one-parameter bifurcation diagram for $\varepsilon = 0.1, k_1 = 0.9, B_0 = 0.207, B_1 = 0.01$, and $\alpha = 0.8$.

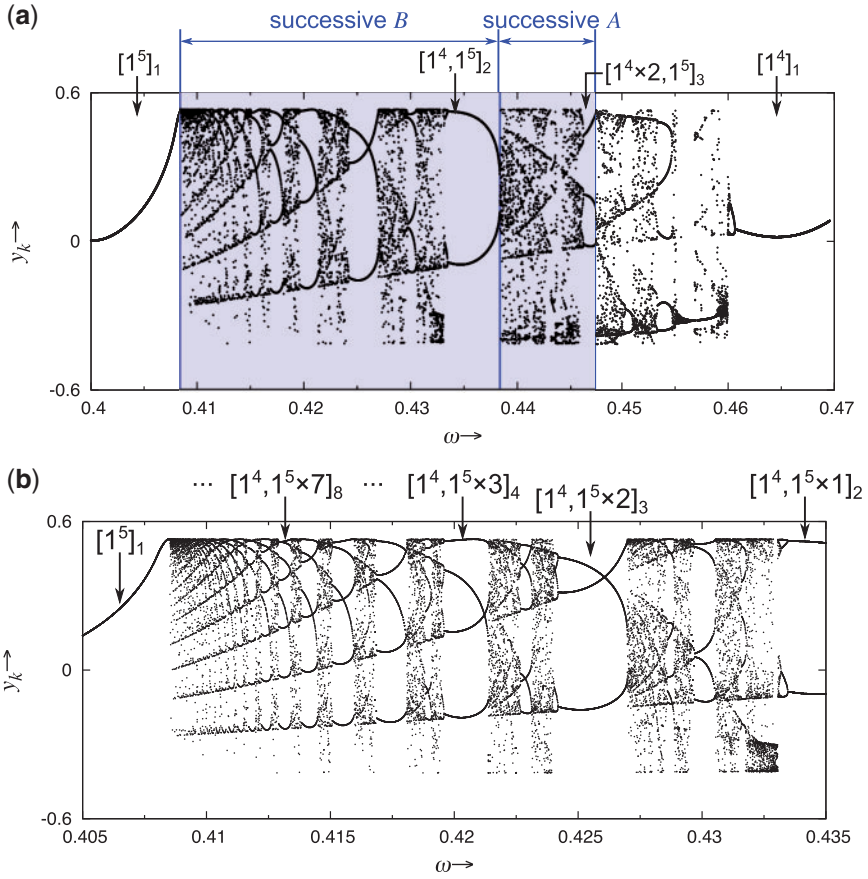

Fig. 6. (a) Magnified view of the one-parameter bifurcation diagram between 1^5 and 1^4. (b) Highly magnified view of (a) for the region labeled "successive B."

MMOIBs (between 1^5 and 1^4) are successively generated many times, the latter ones (between 1^2 and 1^1) only occur a few times.

First, we investigate the MMOs and MMOIBs generated between 1^5 and 1^4. A magnified view of the one-parameter bifurcation diagram is shown in Fig. 6(a). It shows two sets of MMOs and MMOIBs, in the areas marked "successive A" and "successive B," respectively. The concatenation of 1^4 and 1^5 yields a daughter $[1^4, 1^5]_2$, and the concatenation of $[1^4, 1^5]_2$ and 1^4 yields a daughter $[1^4 \times 2, 1^5]_3$. The two sets of MMOIBs begin with $[1^4, 1^5]_2$ and $[1^4 \times 2, 1^5]_3$, respectively.

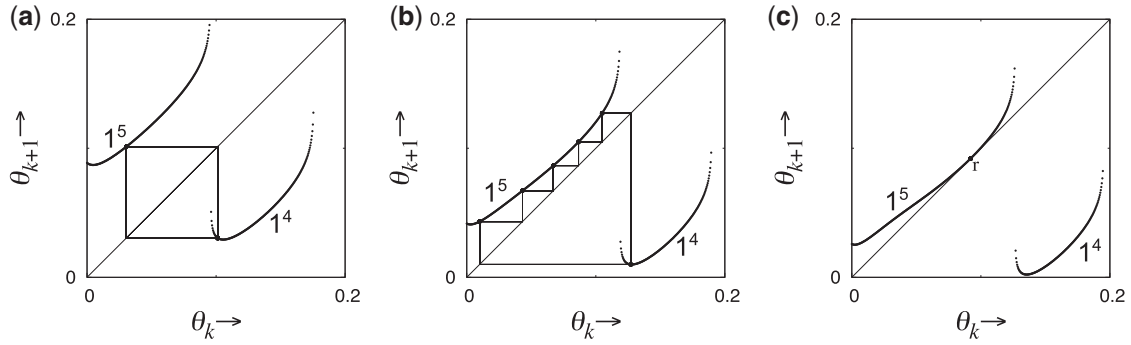

Fig. 7. Magnified views of the Poincaré return maps (a) for $\omega = 0.434$, (b) for $\omega = 0.4155$, and (c) for the MMO increment-terminating tangent bifurcation point with $\omega = 0.408\,505$.

We focus on the MMOIBs that begin with $[1^4, 1^5]_2$, which occurs in the region marked "successive *B*." A highly magnified view of the region marked "successive *B*" in Fig. 6(a) is shown in Fig. 6(b). The trigger sequence for the MMOIBs is $[1^4, 1^5]_2$, as shown in Fig. 7(a). The successive MMOIBs generate the MMO sequences $[1^4, 1^5 \times n]_{n+1}$. Figure 7(b) shows the trajectory for the case $n = 5$. The MMO trajectory strikes the 1^4 branch once and the 1^5 branch five times, and it generates $[1^4, 1^5 \times 5]_6$ corresponding to the MMO time series shown in Fig. 2. The appearance of successive MMOIB-generated MMOs can be clearly seen in Fig. 6(b).

Here, we explain how the successive MMOIBs terminate. We first define an MMO increment-terminating tangent bifurcation at which the MMOIBs accumulate. The MMOIBs can be successively generated many times until they are terminated by an MMO increment-terminating tangent bifurcation, as shown in Fig. 7(c). The MMO increment-terminating tangent bifurcation toward which $[1^4, 1^5 \times n]$ accumulates can be obtained as $\omega = 0.408\,505$. Remember that the branch generating 1^5 is tangent to $\theta_{k+1} = \theta_k$ at a single point r. The shape of the map in the invariant interval that emerges at the bottom left of the θ_k–θ_{k+1} plane suggests that MMOIBs can occur as many times as desired.

Second, we discuss the MMOIBs generated in the region marked "successive *A*," which begins with the MMO sequence $[1^4 \times 2, 1^5]_3$. In this case, the MMOIBs generate the MMO sequence $[1^5, 1^4 \times 2, [1^5, 1^4] \times n]_{2n+3}$ for successive n. The MMO trajectories $[1^5, 1^4 \times 2, [1^5, 1^4] \times 0]_3$, $[1^5, 1^4 \times 2, [1^5, 1^4] \times 1]_5$, $[1^5, 1^4 \times 2, [1^5, 1^4] \times 2]_7$, and $[1^5, 1^4 \times 2, [1^5, 1^4] \times 6]_{15}$ projected on the θ_k–θ_{k+1} plane are shown in Figs. 8(a)–(d), respectively. Note that the MMOIB-generated MMOs in this region converge to $[1^4, 1^5]_2$, at which the two-times composite of the Poincaré map is doubly tangent to $\theta_{k+2} = \theta_k$ at the two points r_1 and r_2, as shown in Fig. 9. Note that this is different from the manner in which MMOIBs are generated in the region marked "successive *B*," and the MMO increment-terminating bifurcation point parameter value is $\omega = 0.438\,340$. The shape of the two-times composite of the Poincaré return map suggests that this type of MMOIB can also occur as many times as desired. Because the 1D Poincaré return map contains two downward-convex branches, the MMOIBs generate asymmetric Farey trees between 1^5 and 1^4, as illustrated in Fig. 10.

Moreover, we have discovered a nested MMOIB bifurcation structure in a short ω interval inside the "successive *B*" region. Figure 11 shows a one-parameter bifurcation diagram between $[1^4, 1^5 \times 1]_2$ and $[1^4, 1^5 \times 2]_3$. A self-similar structure can be observed in this figure. In this interval, we find that $[1^4, 1^5, [1^4, 1^5 \times 2] \times n]_{3n+2}$ occurs for successive n. This result is significant because MMOIBs

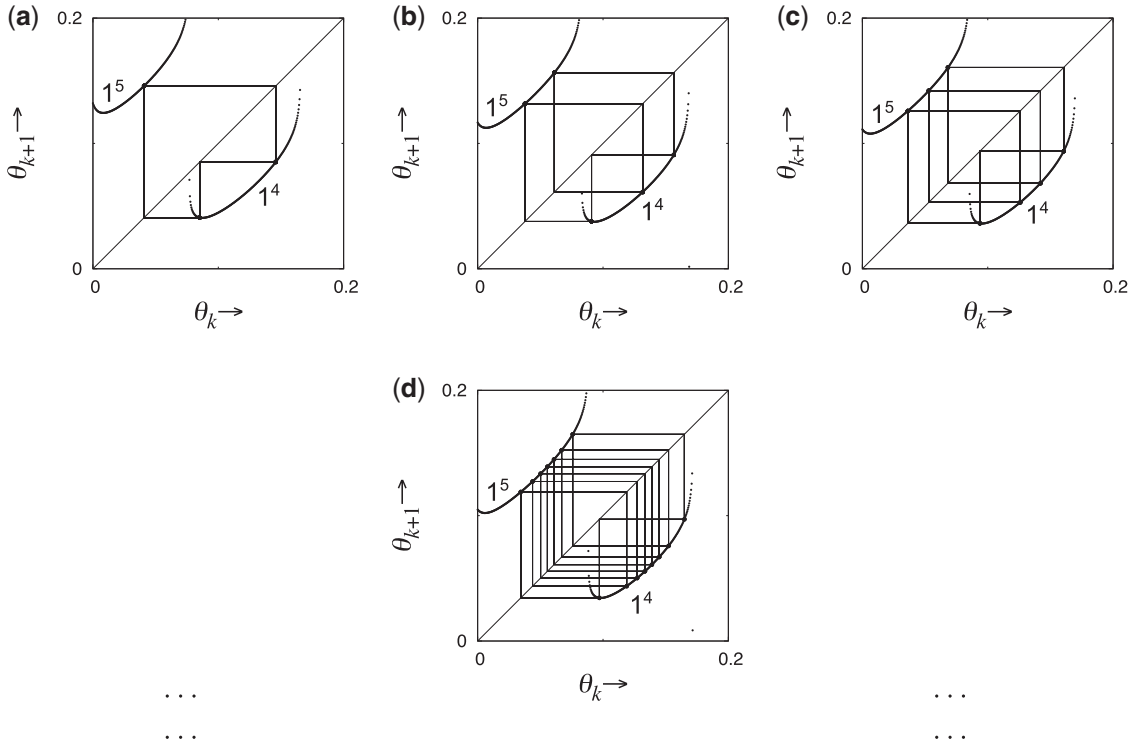

Fig. 8. Magnified views of the Poincaré return maps and complex MMO trajectories for (a) $[1^5, 1^4\times 2, [1^5, 1^4]\times 0]_3$ for $\omega = 0.446\,711$, (b) $[1^5, 1^4 \times 2, [1^5, 1^4] \times 1]_5$ for $\omega = 0.442\,917$, (c) $[1^5, 1^4 \times 2, [1^5, 1^4] \times 2]_7$ for $\omega = 0.441\,363$, and (d) $[1^5, 1^4 \times 2, [1^5, 1^4] \times 6]_{15}$ for $\omega = 0.439\,412$.

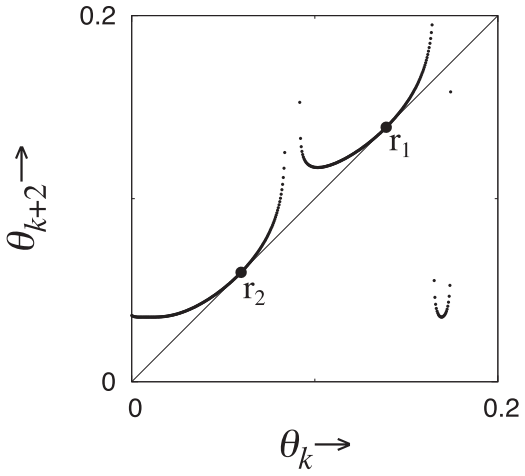

Fig. 9. MMO increment-terminating tangent bifurcation for $[1^5, 1^4 \times 2, [1^5, 1^4] \times n]_{2n+3}$ with $n \to \infty$ ($\omega = 0.438\,340$), for which the two-times composite of the 1D Poincaré map is doubly tangent to the line $\theta_{k+2} = \theta_k$ at r_1 and r_2.

can be nested. Figure 12 shows the $[1^4, 1^5, [1^4, 1^5 \times 2] \times 3]_{11}$ trajectory in the θ_k–θ_{k+1} plane for $\omega = 0.4281$. This type of MMOIB accumulates toward an MMO increment-terminating tangent bifurcation in which T (applied three times) is tangent to the diagonal line $\theta_{k+3} = \theta_k$ at the three points, as shown in Fig. 13 for $\omega = 0.426\,9778$. Such nested MMO bifurcation structures are yet to be reported in the literature on forced MMOIB-generating dynamics [22,23].

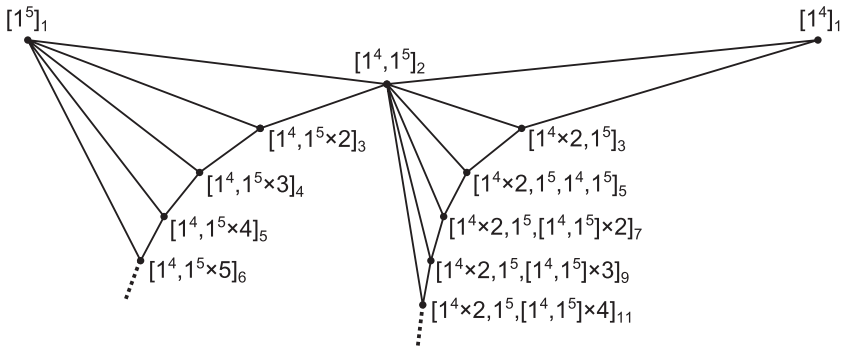

Fig. 10. Asymmetric Farey trees observed between the 1^5 and 1^4 generating regions.

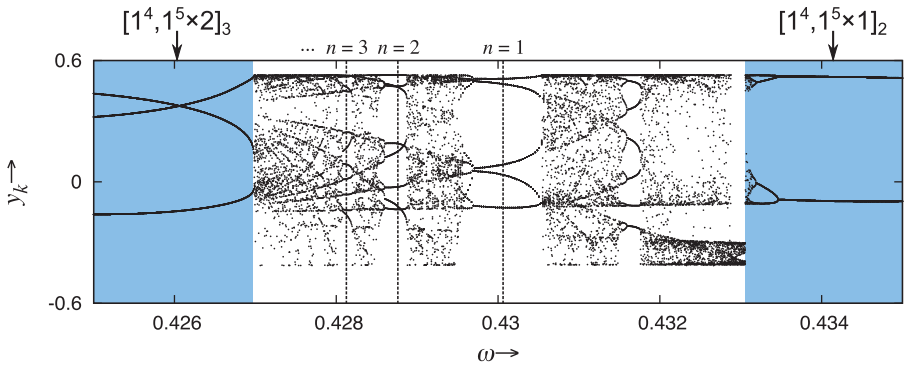

Fig. 11. Nested one-parameter bifurcation diagram obtained between the $[1^4, 1^5 \times 1]_2$ and $[1^4, 1^5 \times 2]_3$ generating regions where $[1^4, 1^5, [1^4, 1^5 \times 2] \times n]_{3n+2}$ occurs successively.

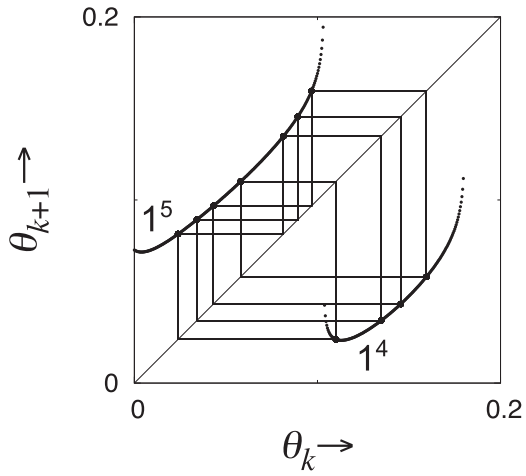

Fig. 12. Trajectories of the MMOs $[1^4, 1^5, [1^4, 1^5 \times 2] \times 3]_{11}$ at $\omega = 0.4281$.

Next, we discuss some cases wherein successive MMOIBs do not occur. A finite number of MMOIBs can be observed between the 1^2 and 1^1 regions, as shown in the one-parameter bifurcation diagrams in Figs. 14(a)–(c). Here, we concentrate on the "FINITE SUCCESSIVE" area in Fig. 14(a), magnified views of which are shown in Figs. 14(b) and (c), respectively. The $[1^1, 1^2 \times n]_{n+1}$ sequence only occurs a few times up to $n = 5$, as shown in Fig. 14(b). Figures 15(a) and (b) show the 1D Poincaré return maps obtained at points Q_1 and Q_2 in Fig. 14(b), respectively. When we decrease the

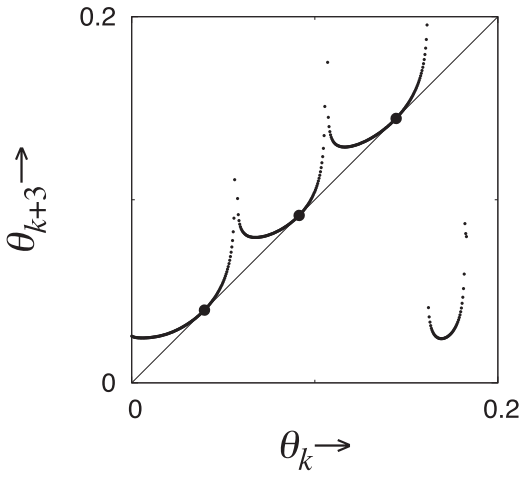

Fig. 13. MMO increment-terminating tangent bifurcation for $[1^4, 1^5, [1^4, 1^5 \times 2] \times n]_{3n+2}$ with $n \to \infty$ ($\omega = 0.426\,9778$), for which the three-times composite of T is tangent to the diagonal line $\theta_{k+3} = \theta_k$ at three points.

bifurcation parameter ω further, the branch generating 1^3 abruptly enters the invariant interval, as shown in Fig. 16(a); this occurs at point Q_3 in Fig. 14(c), where the MMO sequence $[1^1, 1^3, 1^1, 1^2 \times 6]_9$ emerges. As we decrease ω further, the MMO sequences $[1^1, 1^3, 1^1, 1^2 \times n]_{n+3}$ appear for $n = 6$–12, as shown in Fig. 14(c). Figure 16(b) shows the 1D Poincaré return map for $[1^1, 1^3, 1^1, 1^2 \times 12]_{15}$, obtained at point Q_4 in Fig. 14(c), which is an MMO generated by the final MMOIB. MMOIBs cannot continue to emerge for still smaller values of ω. Instead, the invariant interval of the 1D Poincaré return map in the bottom left disappears, as shown in Fig. 16(c.1), (obtained at point Q_5 in Fig. 14(c)), before the branch generating 1^2 touches the line $\theta_{k+1} = \theta_k$ (see Fig. 16(c.2), which is a magnified view of Fig. 16(c.1)). In Fig. 16(c.2), we can clearly see that the map T has a slight gap between the branch generating 1^2 and the line $\theta_{k+1} = \theta_k$. While passing through this slight gap, the solution leaves the bottom left of the Poincaré return map without hitting the branch generating 1^1 and transitions to become a $[2^0]_2$ attractor, which appears in the top right of the map.

4. Firing number, devil's staircase, and chaos

In this section, we introduce the "firing number" F, following past research [5,12]. F is defined as

$$F = \frac{L_N}{L_N + s_N}, \tag{8}$$

where L_N and s_N are the number of large excursions and small peaks, respectively, that are included in one period of the MMO sequence. For example, $F = \frac{1}{1+3} = \frac{1}{4}$ for 1^3, and $F = \frac{1}{1+4} = \frac{1}{5}$ for 1^4. Therefore, F becomes larger if the MMOs include shorter MMO sequences. The firing number for $[1^4, 1^5 \times n]_{n+1}$ is $F = \frac{n+1}{6n+5}$. Therefore, the value of F for $[1^4, 1^5 \times n]_{n+1}$ decreases monotonically with n and asymptotically approaches 1/6. It is known that when the bifurcation parameter is varied, F represents a devil's staircase-like structure [5,12,26]. Devil's staircases of nonautonomous oscillators have previously been reported using the rotation number [23]. In this study, we study the firing number versus ω in MMOs and chaos-generating regions in detail using the 1D Poincaré return map.

Figure 17 shows the one-parameter bifurcation diagram obtained between 1^5 and 1^4 and the corresponding graph of the firing number F. The value of F has been calculated over 70 000 forcing periods for each value of ω. In the one-parameter bifurcation diagram and the graph of the firing number, light blue denotes regions where MMOIB-generated MMOs occur. As mentioned above,

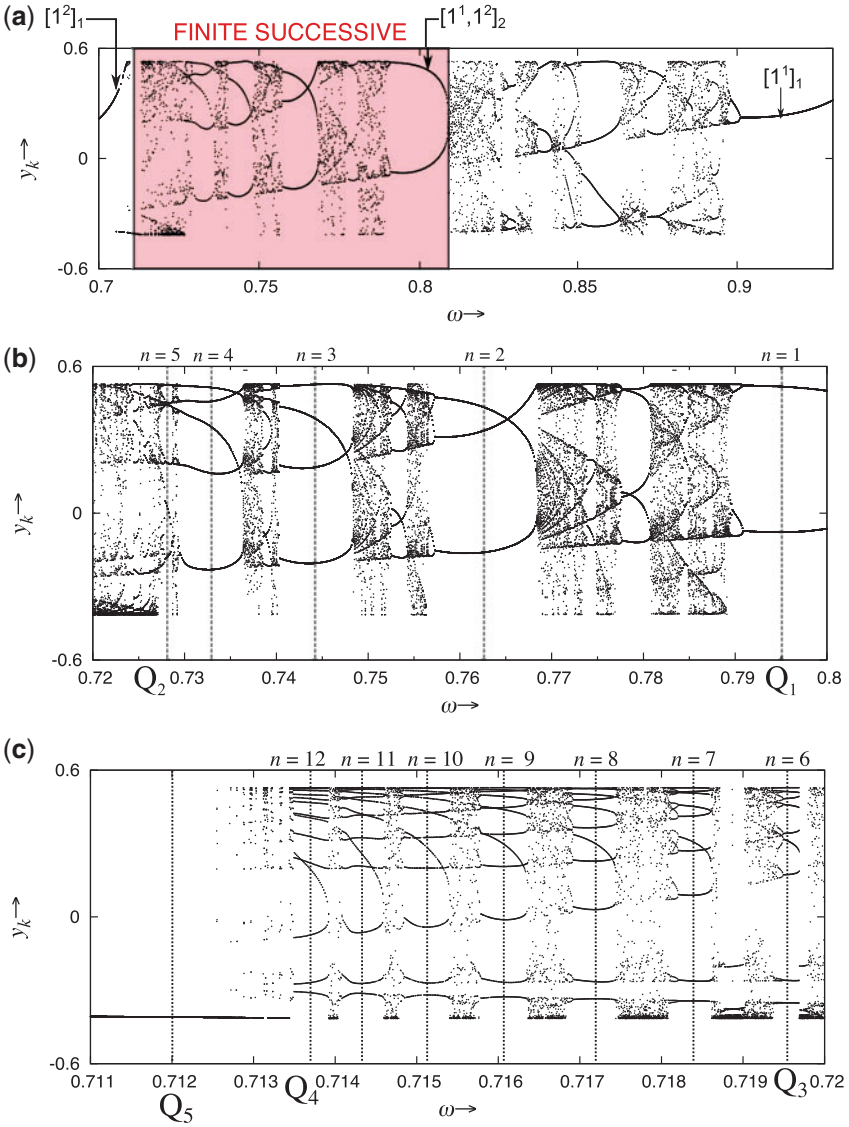

Fig. 14. (a) One-parameter bifurcation diagram between 1^2 and 1^1. (b) Magnified view of (a), where MMOIBs generate the MMOs $[1^1, 1^2 \times n]_{n+1}$ up to $n = 5$. (c) Magnified view of (a) in which the MMOIB-generated MMO sequences include 1^3 as well as 1^1 and 1^2.

F increases monotonically in the light blue regions, and the graph of the firing number represents a devil's staircase-like structure [5,12]. There are cases in which each MMO-generating region caused by an MMOIB overlaps with the hysteresis in the parameter space after several MMOIBs [12]. Therefore, the devil's staircase obtained in such dynamics represents a stepwise function [12,15]. In contrast, each MMO-generating region in this nonautonomous BVP oscillator is sandwiched by chaos.

From Fig. 17, we observed that the firing numbers have higher values in chaos-generating regions in comparison with those in MMO-generating regions marked in light blue. Figure 18(a) shows a magnified view of Fig. 17(b); the corresponding one-parameter bifurcation diagram was previously shown in Fig. 11. The devil's staircase plateaus that can be seen here (regions not marked in light blue in this figure) reveal nested MMO-generating regions represented by $[1^4, 1^5, [1^4, 1^5 \times 2] \times n]_{3n+2}$ for each n, as discussed in the previous section. We can theoretically explain why F takes higher values

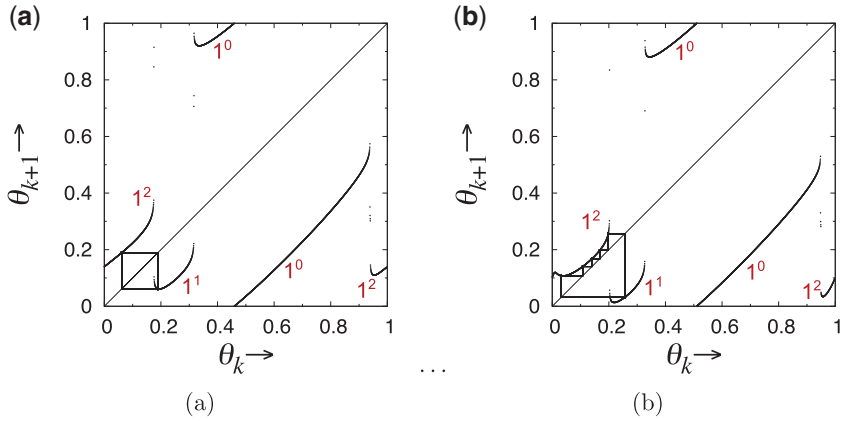

Fig. 15. Poincaré return maps that transition between branches generating 1^2 and 1^1. (a) $[1^1, 1^2]_2$ for $\omega = 0.795$, which is obtained at point Q_1 in Fig. 14(b). (b) The sequence $[1^1, 1^2 \times 5]_6$ for $\omega = 0.7282$, which is obtained at point Q_2 in Fig. 14(b).

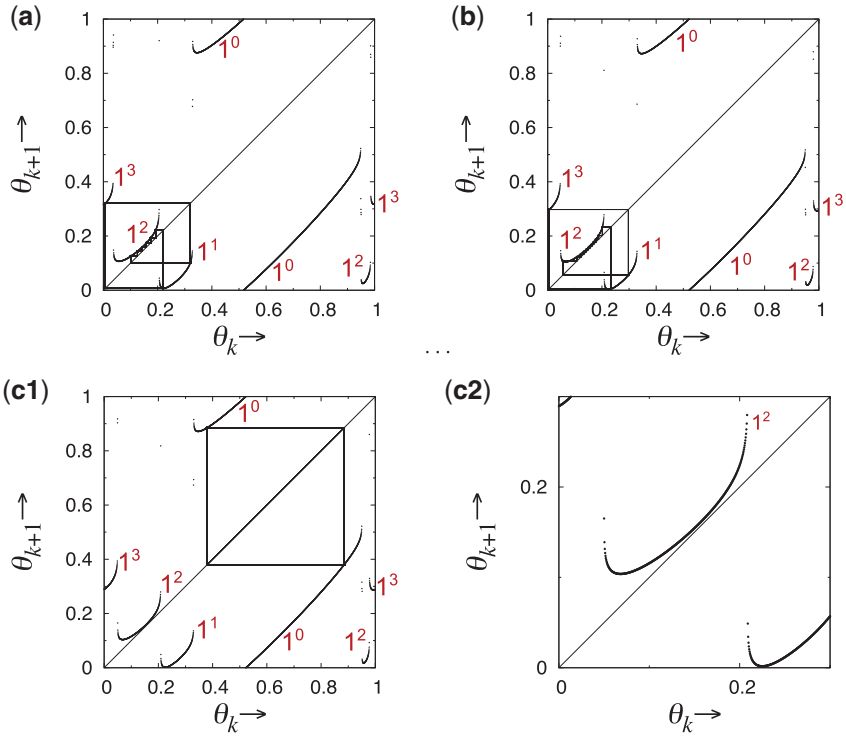

Fig. 16. Poincaré return maps and their trajectories, including the branch generating 1^3. (a) Trajectory $[1^1, 1^3, 1^1, 1^2 \times 6]_9$ in the θ_k–θ_{k+1} plane for $\omega = 0.7196$, which is obtained at point Q_3 in Fig. 14(c). (b) Trajectory $[1^1, 1^3, 1^1, 1^2 \times 12]_{15}$ in the θ_k–θ_{k+1} plane for $\omega = 0.7137$, which is obtained at point Q_4 in Fig. 14(c). (c.1) Sequence $[2^0]_2$ obtained after transitioning from $[1^1, 1^3, 1^1, 1^2 \times 12]_{15}$ for $\omega = 0.712$, which is obtained at point Q_5 in Fig. 14(c). (c.2) Magnified view of (c.1) near the branch 1^2.

in chaos-generating regions. On the left-hand side of Fig. 18(a) (the periodic solution-generating region marked in light blue), the MMO $[1^4, 1^5 \times 2]_3$ is generated and the value of $F = 0.1765$ for $[1^4, 1^5 \times 2]_3$. On the right-hand side of the figure (other periodic solution-generating region marked in light blue), the MMO $[1^4, 1^5]_2$ emerges and the value of $F = 0.1818$ for $[1^4, 1^5 \times 1]_2$. The firing number F takes on lower values in these regions because the waveforms of these MMOs represent longer MMOs, such as 1^4 and 1^5, as shown in Fig. 18(b). In contrast, in the chaos-generating regions,

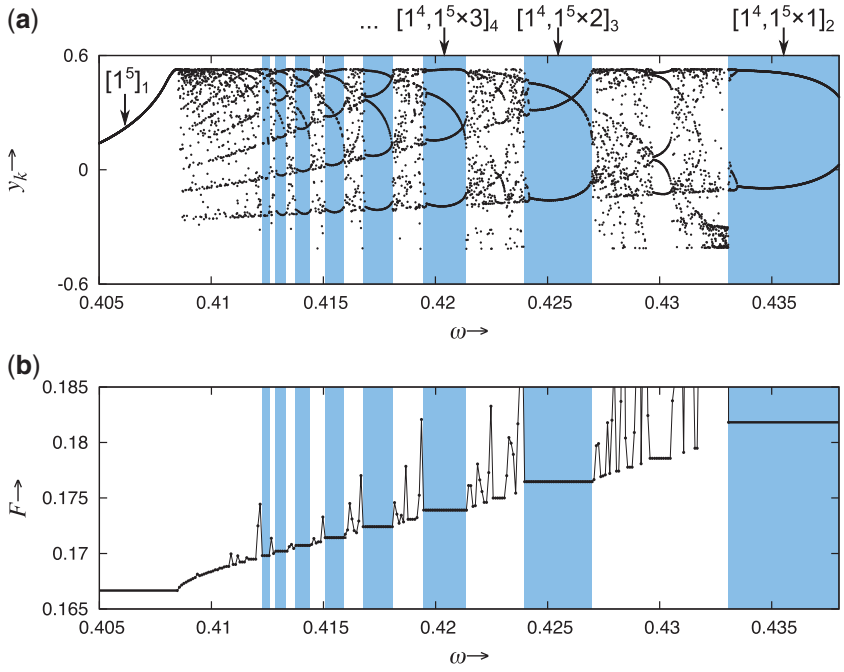

Fig. 17. (a) Magnified view of the one-parameter bifurcation diagram. (b) Firing number F versus ω corresponding to (a), which represents a devil's staircase.

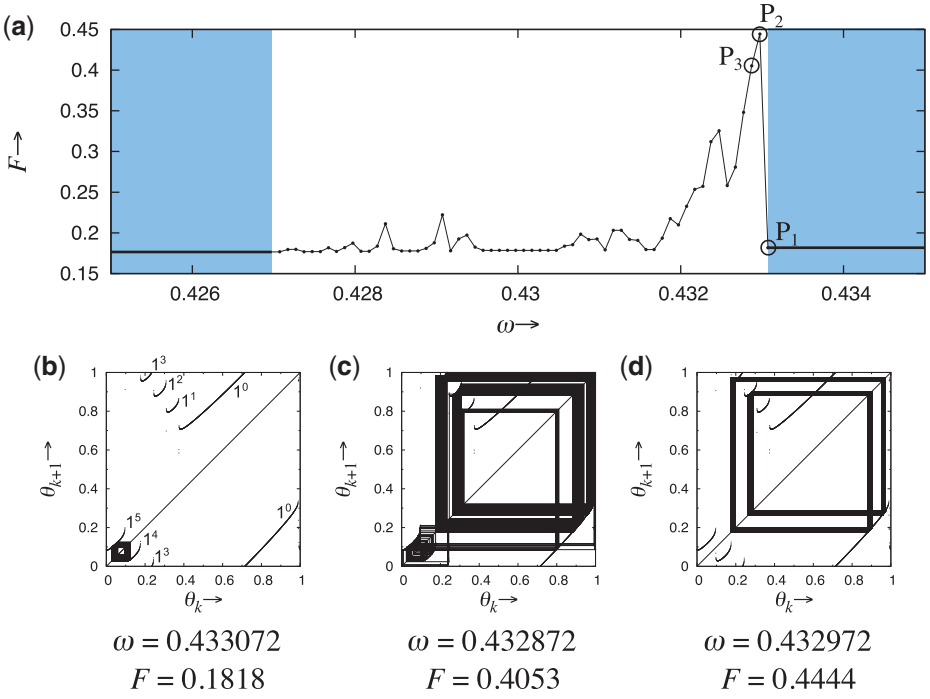

Fig. 18. (a) Magnified view of Fig. 17(b), which corresponds to the nested one-parameter bifurcation diagram shown in Fig. 11. (b) MMO trajectory in the θ_k–θ_{k+1} plane corresponding to point P_1 in (a). (c) Chaotic trajectory in the θ_k–θ_{k+1} plane corresponding to point P_3 in (a). (d) Chaotic trajectory in the θ_k–θ_{k+1} plane corresponding to point P_2 in (a), which repeats the alternating sequence $1^0 \to 1^2 \to 1^0 \to 1^3 \to 1^0$.

F can become larger because the flow strikes the branches that generate shorter MMOs, such as 1^0, 1^2, and 1^3, as shown in Figs. 18(c) and (d). In particular, although the trajectory in Fig. 18(d) is chaotic, it repeats the alternating sequences $[1^0, 1^2, 1^0, 1^3]_4$. The larger values of the firing number F in chaos-generating regions are thus explained theoretically.

5. Conclusion

We investigated MMO bifurcations called MMOIBs generated in a constrained nonautonomous BVP oscillator with a diode, finding two distinct MMOIB types. The MMOIBs observed in the 1^4–1^5 region were successively generated many times, whereas those in the 1^1–1^2 region occurred only a finite number of times. These bifurcation structures were well explained by a 1D Poincaré return map derived from a constrained dynamical oscillator. In particular, we rigorously defined the MMO increment-terminating tangent bifurcations toward which successively generated MMOIBs accumulate and numerically derived these bifurcation points. We also discovered nested MMOIB-generated MMOs in a short interval in the 1^4–1^5 region. In addition, we created a graph of the firing number, which represents a devil's staircase. We observed the chaotic windows between the neighboring MMOIB-generated MMOs and found that in the chaos-generating region, the value of the firing number was higher compared to that in the MMO-generating regions, which we explained using 1D Poincaré return maps. In future research, we plan to comprehensively investigate the nested bifurcation structures of the MMOIBs generated by this BVP oscillator.

Acknowledgements

This work was supported by Japan Society for the Promotion of Science (JSPS) KAKENHI Grant Numbers 16H02876 and 16K06430 and by RSF Grant Number 17-12-01008.

References

[1] M. Brøns, T. J. Kaper, and H. G. Rotstein, Chaos **18**, 015101 (2008).
[2] M. Brons, M. Krupa, and M. Wechselberger, Fields Inst. Commun. **49**, 39 (2006).
[3] H. L. Swinney, Physica D **7**, 3 (1983).
[4] I. R. Epstein, Physica D **7**, 47 (1983).
[5] S. K. Scott, *Chemical Chaos* (Oxford University Press, Oxford, UK, 1993).
[6] J. L. Hudson, M. Hart, and D. Marinko, J. Chem. Phys. **71**, 1601 (1979).
[7] M. Orban and I. R. Epstein, J. Phys. Chem. **86**, 3907 (1982).
[8] J. Maselko and H. L. Swinney, J. Chem. Phys. **85**, 6430 (1986).
[9] F. N. Albahadily, J. Ringland, and M. Schell, J. Chem. Phys. **90**, 813 (1989).
[10] T. Yoshinaga, H. Kawakami, and K. Yoshikawa, IEICE Trans. Fund. Electron. Comm. Comput. Sci. **J71-A**, 1843 (1988) [in Japanese].
[11] H. Kawakami, IEEE Trans. Circuits Syst. **31**, 248 (1984).
[12] V. Petrov, S. K. Scott, and K. Showalter, J. Chem. Phys. **97**, 6191 (1992).
[13] M. Krupa, N. Popović, and N. Kopell, SIAM J. Appl. Dyn. Syst. **7**, 361 (2008).
[14] M. Sekikawa, N. Inaba, T. Yoshinaga, and T. Hikihara, Phys. Lett. A **374**, 3745 (2010).
[15] A. L. Kawczyński, V. O. Khavrus, and P. E. Strizhak, Chaos **10**, 299 (2000).
[16] K. Shimizu, M. Sekikawa, and N. Inaba, Phys. Lett. A **375**, 1566 (2011).
[17] K. Shimizu, Y. Saito, M. Sekikawa, and N. Inaba, Physica D **241**, 1518 (2012).
[18] K. Shimizu, M. Sekikawa, and N. Inaba, Chaos **25**, 023105 (2015).
[19] K. Shimizu and N. Inaba, Prog. Theor. Exp. Phys. **2016**, 033A01 (2016).
[20] T. Kousaka, Y. Ogura, K. Shimizu, H. Asahara, and N. Inaba, Physica D **353–354**, 48 (2017).
[21] E. Kutafina, Comp. Appl. Math. **34**, 81 (2015).
[22] G. Markman and K. Bar-Eli, J. Phys. Chem. **98**, 12248 (1994).
[23] M. Brøns, P. Gross, and K. Bar-Eli, Int. J. Bifurc. Chaos **7**, 2621 (1997).
[24] P. De Maesschalck, E. Kutafina, and N. Popović, J. Dyn. Diff. Equat. **26**, 955 (2014).

[25] J. G. Freire and J. A. C. Gallas, Phys. Lett. A **375**, 1097 (2011).
[26] J. G. Freire and J. A. C. Gallas, Phys. Chem. Chem. Phys. **13**, 12191 (2011).
[27] J. G. Freire, M. R. Gallas, and J. A. C. Gallas, in *Chaotic, Fractional, and Complex Dynamics: New Insights and Perspectives*, eds. M. Edelman, E. E. N. Macau, and M. A. F. Sanjuan (Springer, 2017), p. 101.
[28] M. J. B. Hauser and J. A. C. Gallas, J. Phys. Chem. Lett. **5**, 4187 (2014).
[29] J. Guckenheimer and C. Scheper, SIAM J. Appl. Dyn. Syst. **10**, 92 (2011).
[30] M. Desroches, J. Guckenheimer, B. Krauskopf, C. Kuehn, H. M. Osinga, and M. Wechselberger, SIAM Rev. **54**, 211 (2012).
[31] M. Desroches, T. J. Kaper, and M. Krupa, Chaos **23**, 046106 (2013).
[32] M. Krupa, B. Ambrosio, and M. A. Aziz-Alaoui, Nonlinearity **27**, 1555 (2014).
[33] M. Krupa, A. Vidal, M. Desroches, and F. Clément, SIAM J. Appl. Dyn. Syst. **11**, 1458 (2012).
[34] J. Rubin and M Wechselberger, Chaos **18**, 015105 (2008).
[35] A. Roberts, E. Widiasih, M. Wechselberger, and C. K. R. T. Jones, Physica D **292**, 70 (2015).
[36] A. Pikovsky, M. Rosemblum, and J. Kurths, *Synchronization: A Universal Concept in Nonlinear Science* (Cambridge University Press, Cambridge, UK, 2001).
[37] V. S. Anishchenko, T. E. Vadivasova, D. E. Postnov, and M. A. Safonova, Int. J. Bifurc. Chaos **2**, 633 (1992).
[38] V. Astakhov, M. Hasler, T. Kapitaniak, A. Shabunin, and V. Anishchenko, Phys. Rev. E **58**, 5620 (1998).
[39] H. Broer, C. Simó, and R. Vitolo, Bull. Belg. Math. Soc. Simon Stevin **15**, 769 (2008).
[40] C. Baesens, J. Guckenheimer, S. Kim, and R. S. MacKay, Physica D **49**, 387 (1991).
[41] A. P. Kuznetsov and Y. V. Sedova, Int. J. Bifurc. Chaos **24**, 1430022 (2014).
[42] N. V. Stankevich, J. Kurths, and A. P. Kuznetsov, Commun. Nonlinear Sci. Numer. Simulat. **20**, 316 (2015).
[43] Y. P. Emelianova, A. P. Kuznetsov, L. V. Turukina, I. R. Sataev, and N. Y. Chernyshov, Commun. Nonlinear Sci. Numer. Simulat. **19**, 1203 (2014).
[44] T. Saito, IEEE Trans. Circuits Syst. **35**, 1147 (1988).
[45] E. Köksal Ersöz, M. Desroches, and M. Krupa, Physica D **349**, 46 (2017).
[46] E. Köksal Ersöz, M. Desroches, M. Krupa, and F. Clément, SIAM J. Appl. Dyn. Syst. **15**, 580 (2016).
[47] N. Inaba and M. Sekikawa, Nonlinear Dyn. **76**, 1711 (2014).
[48] M. Sekikawa, K. Shimizu, N. Inaba, H. Kita, T. Endo, K. Fujimoto, Tetsuya Yoshinaga, and K. Aihara, Phys. Rev. E **84**, 056209 (2011).
[49] J. Nagumo, S. Arimoto, and S. Yoshizawa, Proc. IRE **50**, 2061 (1962).
[50] T. Nomura, S. Sato, S. Doi, J. P. Segundo, and M. D. Stiber, Biol. Cybern. **69**, 429 (1993).
[51] T. Nomura, S. Sato, S. Doi, J. P. Segundo, and M. D. Stiber, Biol. Cybern. **72**, 55 (1994).
[52] S. Sato and S. Doi, Math. Biosci. **112**, 243 (1992).
[53] S. Doi and S. Sato, Math. Biosci. **125**, 229 (1995).
[54] R. M. May, Nature **261**, 459 (1976).
[55] P. Collet and J. P. Eckmann, *Iterated Maps on the Interval as Dynamical Systems* (Birkhäuser, Basel, 1980).
[56] Y. Katznelson, J. Anal. Math. **31**, 1 (1977).
[57] S. Ostlund, D. Rand, J. Sethna, and E. Siggia, Physica D **8**, 303 (1983).
[58] T. Y. Li and J. A. Yorke, Trans. Am. Math. Soc. **235**, 183 (1978).
[59] A. Lasota and J. A. Yorke, Trans. Am. Math. Soc. **186**, 481 (1973).
[60] T.-Y. Li and J. A. Yorke, Am. Math. Month. **82**, 985 (1975).
[61] V. Avrutin and M. Schanz, Nonlinearity **19**, 531 (2006).
[62] V. Avrutin, A. Granados, and M. Schanz, Nonlinearity **24**, 2575 (2011).
[63] B. Schenke, V. Avrutin, and M. Schanz, Proc. R. Soc. Lond. A **467**, 1503 (2011).
[64] A. Granados, L. Alsedá, and M. Krupa, SIAM Rev. **59**, 225 (2017).
[65] A. Rabinovitch and I. Rogachevskii, Chaos **9**, 880 (1999).
[66] A. Rabinovitch, R. Thieberger, M. Friedman, and S. Goshen, Chaos Solitons Fractals **7**, 1713 (1996).